Effect of Salt and pH on the Activation of Photoactive Yellow Protein and Gateway Mutants Y98Q and Y98F†

Berthold Borucki,‡ John A. Kyndt,§ Chandra P. Joshi,‡ Harald Otto,‡ Terry E. Meyer,§ Michael A. Cusanovich,§ and Maarten P. Heyn*,‡

Biophysics Group, Department of Physics, Freie Universität Berlin, Arnimallee 14, 14195 Berlin, Germany, and Department of Biochemistry and Molecular Biophysics, University of Arizona, Tucson, Arizona 85721

Received May 26, 2005; Revised Manuscript Received August 23, 2005

ABSTRACT: We investigated the photocycle of mutants Y98Q and Y98F of the photoactive yellow protein (PYP) from *Halorhodospira halophila*. Y98 is located in the $\beta_4-\beta_5$ loop and is thought to interact with R52 in the $\alpha_3-\alpha_4$ loop thereby stabilizing this region. Y98 is conserved in all known PYP species, except in Ppr and Ppd where it is replaced by F. We find that replacement of Y98 by F has no significant effect on the photocycle kinetics. However, major changes were observed with the Y98Q mutant. Our results indicate a requirement for an aromatic ring at position 98, especially for recovery and a normal I_1/I_2 equilibrium. The ring of Y98 could stabilize the $\beta_4-\beta_5$ loop. Alternatively, the Y98 ring could transiently interact with the isomerized chromophore ring, thereby stabilizing the I_2 intermediate in the I_1/I_2 equilibrium. For Y98Q, the decay of the signaling state I_2' was slowed by a factor of ∼40, and the rise of the I_2 and I_2' intermediates was slowed by a factor of 2−3. Moreover, the I_1 intermediate is in a pH-dependent equilibrium with I_2/I_2' with the ratio of the I_1 and I_2 populations close to one at pH 7 and 50 mM KCl. From pH 5.5 to 8, the equilibrium shifts toward I_1, with a pK_a of ∼6.3. Above pH 8, the populations of I_1 and I_2/I_2' decrease due to an equilibrium between I_1 and an additional species I_1' which absorbs at ∼425 nm (pK_a ∼ 9.8) and which we believe to be an I_2-like form with a surface-exposed deprotonated chromophore. The $I_1/I_2/I_2'$ equilibrium was found to be strongly dependent on the KCl concentration, with salt stabilizing the signaling state I_2' up to 600 mM KCl. This salt-induced transition to I_2' was analyzed and interpreted as ion binding to a specific site. Moreover, from analysis of the amplitude spectra, we conclude that KCl exerts its major effect on the I_2 to I_2' transition, i.e., the global conformational change leading to the signaling state I_2' and the exposure of a hydrophobic surface patch. In wild type and Y98F, the I_1/I_2 equilibrium is more on the side of I_2/I_2' as compared to Y98Q but is also salt-dependent at pH 7. The I_2 to I_2' transition appears to be controlled by an ionic lock, possibly involving the salt bridge between K110 on the β-scaffold and E12 on the N-terminal cap. Salt binding would break the salt bridge and weaken the interaction between the two domains, facilitating the release of the N-terminal domain from the β-scaffold in the formation of I_2'.

Photoactive yellow protein (PYP)[1] is a bacterial photoreceptor that was initially isolated from *Halorhodospira halophila* (*1*, *2*) and has since been detected in six other organisms (*3*). Recently, it has been found as a module in the multidomain chimeric proteins PYP-phytochrome-related (Ppr) and PYP/phytochrome/diguanylate cyclase (Ppd), which have two chromophore domains, a PYP and a bacteriophytochrome domain (*3*−*5*).

PYP is the prototype of a structural motif termed the PAS domain, which is found in a large and widely distributed class of sensory proteins that respond to a diverse range of compounds and stimuli (*3*, *6*, *7*). The structure, function, and dynamics of PYP have recently been reviewed (*6*, *8*).

PYP is an attractive model system to study signal transduction because high-resolution structures are available for the dark state (*9*) and some of the photocycle intermediates (*10*, *11*). The blue light absorption of PYP (λ_{max} = 446 nm) is due to its 4-hydroxycinnamoyl chromophore that is bound via a thioester linkage to cysteine 69. In the dark state P, the anionic form of the chromophore is stabilized by hydrogen bonds to E46 and Y42, and the 7−8 double bond is trans. Photoexcitation is followed by rapid isomerization around this bond (*12*) and a subsequent photocycle consisting of a number of spectrally distinguishable intermediates (*2*, *13*). The first long-lived intermediate, I_1, follows the two very short-lived intermediates I_0 and $I_0^‡$. It forms in about 3 ns, has a red-shifted absorption spectrum (λ_{max} = 460 nm), is still hydrogen-bonded to Y42 and E46, and has a deprotonated chromophore. Conversion of I_1 to the signaling state occurs in two steps. First, the chromophore is protonated in the formation of the I_2 intermediate (200−300 μs), thereby

† This work was supported by NIH Grant GM 66146 (to M.A.C.) and DFG Grant GK 788 TP A9 (to M.P.H.).

* Corresponding author. E-mail: heyn@physik.fu-berlin.de. Fax: +49-30-8385 6299. Phone: +49-30-8385 6160.

‡ Freie Universität Berlin.

§ University of Arizona.

[1] Abbreviations: SVD, singular value decomposition; PYP, photoactive yellow protein; PAS domain, acronym formed from the names of the first three proteins recognized as sharing this sensory domain; Ppr, PYP-phytochrome-related; Ppd, PYP/phytochrome/diguanylate cyclase.

10.1021/bi050991z CCC: $30.25
Published on Web 09/27/2005

blue-shifting the absorption spectrum ($\lambda_{max} \sim 355$ nm). In the second step, occurring in about 2−3 ms, a global conformational change leads to the putative signaling state I_2'. Structural studies show that either in I_2' or in I_2 the chromophore ring swings out toward the surface (*10*, *11*). Whether the chromophore is protonated intramolecularly from E46 (*14*), or from the external medium (*15*), remains to be established. At least for the mutants E46Q and E46A, it was shown that the chromophore is protonated from the solvent (*15*) with high efficiency and faster than in wild type.

The I_2 to I_2' transition, the formation of the signaling state, is associated with a global conformational change, which has also been described as partial unfolding with exposure of a hydrophobic surface patch (*16*). The structural evidence comes from high-resolution NMR (*17*, *18*), time-resolved FTIR (*14*, *19*), CD (*20*, *21*), and small-angle X-ray scattering (*20*, *22*). Kinetic evidence was provided by dye-binding experiments which showed that hydrophobic dyes bind transiently to I_2' but not to I_2 (*15*, *23*). The evidence for a major conformational change comes from studies with PYP in aqueous solution. Interestingly, no large structural changes have been detected in I_2 or I_2' by high-resolution X-ray diffraction (*11*). They are presumably prevented by packing constraints in the crystal lattice. FTIR measurements on powder samples of crystalline PYP indicate that the conformational changes during I_2' formation are strongly suppressed and that E46 remains protonated (*14*, *24*). It is therefore questionable whether the crystal structures of intermediates beyond I_2 are relevant for understanding the mechanism in solution. The observation, that large structural changes do not occur in crystals, is not limited to PYP. It was recently shown by FTIR that formation of the active state of rhodopsin, M_{II}, is blocked in two-dimensional crystals (*25*).

One of the outstanding questions concerning the mechanism of PYP is how the light-induced isomerization of the chromophore triggers the structural change. The initial structural perturbation is localized in the chromophore binding pocket on one side of the central β-scaffold. However, the global conformational change appears to occur on the other side of the β-scaffold, mainly in the N-terminal domain (*17*). This segment of residues 1−28 forms a separate subdomain in the PYP structure that is packed against the central β-sheet (*9*). How the signal is transmitted from the signal detection domain across the central β-sheet to the N-terminal domain remains a key question. Various hypotheses have been proposed for this long-range interaction, among them the hydrophobic collapse model (*6*), the protein quake model (*14*, *26*), and more recently a helix-capping model (*11*). In the hydrophobic collapse model, the hydrophobic pocket vacated by the isomerized chromophore collapses upon itself, distorting the central β-sheet and weakening its interaction with the N-terminal domain. This leads to exposure of a hydrophobic surface at the N-terminus-central β-sheet interface, which provides a binding site for interaction partners. The interaction between the β-scaffold and N-terminal cap thus plays a major role. It has focused attention on the role of the interface between these two domains, which are held together in the dark state by hydrophobic and electrostatic interactions (*9*, *27*). In I_2' these two domains are believed to move apart, leading for example to a larger radius of gyration (*20*, *22*). In the protein quake model, the transfer of a proton from E46 to the chromophore is proposed to trigger the global conformational changes that result in the formation of the signaling state (*14*). Recently, a helix-capping model has been described (*11*), whereby the signal is propagated to the N-terminus through breakage of the hydrogen bonds between the chromophore and E46 and Y42, which results in a small movement of helix B. That, in turn, results in breakage of hydrogen bonds between N43 also located in helix B and the backbone of F28 and L23 in the N-terminal helices. The loss of hydrogen bonds between N43 and E46 as well as that between D24 and A44 further weaken the interaction of the N-terminus with the remainder of the protein.

It was recently realized that the photocycle of PYP is not unidirectional but involves equilibria, back reactions, and branching (*28*, *29*). It was shown that I_1 and I_2 are in a pH-dependent equilibrium at alkaline pH in wild type (*28*) and at neutral pH in the mutants E46Q and E46A (*28*), with the equilibrium shifting to I_1 at higher pH. I_1 and I_2 thus coexist and decay together in the return to the dark state P. The existence of this equilibrium was confirmed for wild type at alkaline pH in later work (*30*). The similarity to the pH-dependent M_I/M_{II} equilibrium in the activation of rhodopsin has been pointed out (*28*), where high pH favors M_I, the inactive precursor of the signaling state. A similar pH-dependent equilibrium of intermediates was also described in *Thermochromatium tepidum* PYP (*5*). We recently showed, using time-resolved photoreversal measurements, that I_2 and I_2' are also in equilibrium (*31*). These conformational equilibria play an important role and are of great interest because parameters that shift and control these equilibria should provide information on the mechanism of generation of the active state I_2'.

Studies with proteins mutated at E46, Y42, R52, and M100 or with N-terminal truncations have provided valuable insights into the mechanism of PYP. Here we investigate amino acid substitutions at position 98. Y98 is conserved in five out of seven known PYP species. In the other two (Ppr and Ppd), it is replaced by F, another residue with an aromatic ring. Y98 is located in the $\beta_4-\beta_5$ loop that is believed to interact with the $\alpha_3-\alpha_4$ loop, stabilizing their structure. Whereas crystallographic work has identified a hydrogen bond between R52 (in loop $\alpha_3-\alpha_4$) and the backbone carbonyl of Y98 (*9*), NMR spectroscopy suggests an interaction between the guanidinium group of R52 and the Y98 ring structure (*32*). The diffraction studies suggest that in I_2 R52 forms a new hydrogen bond with the chromophore (*10*). Y98 is close to M100 in the $\beta_4-\beta_5$ loop, and mutations of M100 have been shown to have dramatic effects on the photocycle, slowing down the decay of I_2 by 3 orders of magnitude (*20*, *33*). On the basis of the high resolution X-ray structures of the dark state P, it was recently suggested that Y98 and P68 could interfere sterically with the trans/cis isomerization (*34*). It was proposed that concerted motions of Y98 and P68 were necessary for the chromophore to pass through a gate formed by these residues (*34*); thus, Y98Q and Y98F are appropriately termed "gateway" mutants.

MATERIALS AND METHODS

Protein Production and Purification. H. halophila holo-PYP was produced by the use of the biosynthetic enzymes TAL and pCL and subsequently purified from *Escherichia*

coli BL21(DE3) as described (*35*). The mutagenesis was performed as described (*36*).

Transient Absorption Spectroscopy. These measurements and their analysis were performed as described previously (*37*). The amplitude spectra $B_i(\lambda)$ in

$$\Delta A(t,\lambda) = \sum_i B_i(\lambda)\, e^{-t/\tau_i} + B_0(\lambda) \qquad (1)$$

were constructed, following SVD analysis, as in ref *38*. Intermediate spectra were calculated according to ref *37*.

Salt Binding. The effect of salt on the I_1/I_2' conformational equilibrium was modeled by analogy to the corresponding case for the M_I/M_{II} equilibrium of rhodopsin (*39*). The binding data were fitted with the following function (*39*):

$$[I_2]/([I_2] + [I_1]) = C^n/(C^n + K^n) \qquad (2)$$

which describes the salt dependence of the fraction of the I_1/I_2 equilibrium in the I_2 state. C is the salt concentration, K is the dissociation constant, and n is the Hill coefficient. This model assumes that when salt binds to PYP in the I_1 state, it is converted to the structurally altered signaling state I_2' with protonated chromophore. Salt binding thus converts the "closed/locked" structure of I_1 to the "open/unlocked" structure of I_2'. "Open" and "closed" refer to structural states with the N-terminal domain attached to or detached from the β-scaffold. "Locked" and "unlocked" refer to the presence or the absence of a salt linkage (see discussion).

In most of our experiments, the I_1 and I_2 concentrations were deduced from transient absorption measurements at a few wavelengths (500 and 490 nm for I_1; 350 nm for I_2 and I_2'). Since the spectra of I_2 and I_2' are quite similar, we could not distinguish between I_2 and I_2' from measurements at 350 nm alone. Therefore, in our measurements of the pH and salt dependence of the I_1/I_2 equilibrium, we measure the sum of the I_2 and I_2' populations. We will designate this by writing I_2/I_2' instead of I_2. For a few selected conditions of pH and salt, we measured the photocycle across the complete spectrum. From these data, we could derive the amplitude spectra for each transition, and on this basis we can distinguish between I_2 and I_2'.

RESULTS

Photocycles of Y98Q, Y98F, and Wild Type. Figure 1 shows time traces for the photocycles of Y98Q, Y98F, and wild type at the three diagnostic wavelengths, 450 nm (A), 350 nm (B), and 500 nm (C) at pH 7.0 and 50 mM KCl. Note the logarithmic time scale ranging over more than 8 decades of time from 100 ns to 20 s. The depletion signal at 450 nm reflects the initial amount of bleach due to the formation of I_1 (at 100 ns) as well as provides kinetic information on the formation and decay of I_2 and I_2'. The signal at 350 nm primarily monitors the formation and decay of I_2 and I_2', which have similar spectra. The signal at 500 nm is mainly due to the I_1 intermediate. In Figure 1, the time traces for wild type, Y98F, and Y98Q are scaled so that the initial absorbance change at 450 nm is the same in all three cases (panel A). This is correct if the spectra of P and I_1 are identical for all three proteins, which is approximately true (data not shown). Panels A and B show that the kinetics of formation and decay of I_2 are very similar

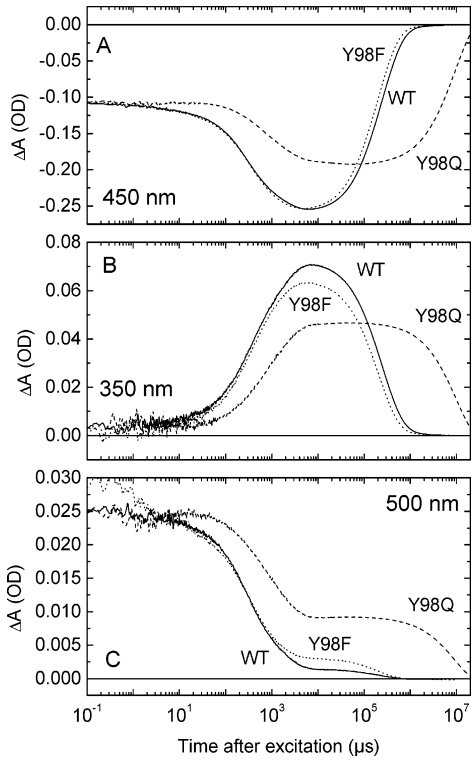

FIGURE 1: Transient absorption changes of PYP WT (solid lines) and the mutants Y98Q (dashed lines) and Y98F (dotted lines), after laser flash excitation at 430 nm measured at three characteristic wavelengths: (A) 450 nm, (B) 350 nm, and (C) 500 nm. The traces are averages of 60 scans. Conditions: 50 mM Tris buffer, 50 mM KCl, pH 7.0, 20 °C, protein concentration = 34 μM.

in wild type and Y98F. I_2 is formed from I_1 in ~280 μs (τ_1) and decays to I_2' in 2.0 ms (τ_2). I_2' reverts to the initial dark state P in 260 ms (τ_3). However, the formation of I_2 is delayed to ~620 μs in Y98Q. Moreover, the amount of I_2/I_2' formed (panel B) is significantly less than in Y98F and wild type. The recovery of the ground state P in Y98Q is dramatically slowed from ~260 ms to 9.5 s. The traces in panel C monitor the decay of I_1 at 500 nm. At this wavelength, it is apparent that the kinetic traces for wild type and Y98F also contain a fourth decay component with a time constant of a few microseconds (τ_f). The trace for wild type shows that the I_1 population does not decay to zero in the I_1 to I_2 transition (panel C) but that a small amount of I_1 remains after several milliseconds, which decays together with I_2' in 260 ms. For Y98F, the situation is similar, except that the population of I_1 remaining at 10 ms is larger than in the case of wild type (panel C). In Y98F there is, compared to wild type, less I_2/I_2' (panel B) and more I_1 (panel C) after 10 ms. For Y98Q, the amount of I_1 remaining after the transitions to I_2 and I_2' and decaying in parallel with I_2' is very large (Figure 1C). Moreover, the population of I_2/I_2' is correspondingly reduced (panel B). These data show clearly that I_1, I_2, and I_2' are in equilibrium and decay together at pH 7.0. This equilibrium is apparently far on the side of the two I_2 species in wild type and Y98F and is shifted strongly toward I_1 in the mutant Y98Q. The time constants from a global fit of the data of Figure 1 and of time traces at 8−16 additional wavelengths with four exponentials are presented in Table 1.

pH Dependence of the Y98Q Photocycle. To learn more about the I_1/I_2 equilibrium in Y98Q, we studied its pH

Table 1: Time Constants of Photocycle Kinetics[a]

	τ_f, μs	τ_1, μs	τ_2, ms	τ_3, ms
wild type	5.9	280	2.0	260
Y98Q	7.8	620	3.5	9500
Y98F	6.5	290	1.7	210

[a] The SVD time traces were fitted with a sum of exponentials, τ_i are the corresponding time constants; conditions: pH 7.0, 50 mM KCl, 20 °C.

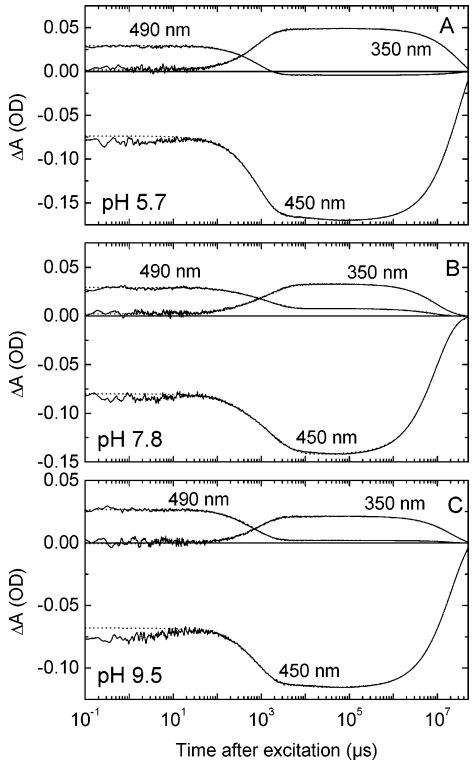

FIGURE 2: Transient absorption changes of the mutant Y98Q after laser flash excitation at 430 nm measured at the three wavelengths 450, 350, and 490 nm, as indicated. (A) pH 5.7, (B) pH 7.8, (C) pH 9.5. The traces are averages of 20 scans. Conditions: 50 mM Tris buffer, 50 mM KCl, 20 °C, protein concentration = 23 μM. The dotted lines are simultaneous fits to the traces at 450, 350, 490, and 500 nm (data not shown) with three exponentials in the time range from 20 μs to 50 s.

dependence. In previous work with E46Q, E46A, and wild type, we showed that these equilibria are strongly pH dependent (*28*). The photocycle kinetics were measured at 50 mM KCl from pH 5.5 to 10.1. At each pH value, the transient absorbance differences were detected at four diagnostic wavelengths of 500 and 490 nm for I_1, 350 nm for I_2 and I_2', and 450 nm for the depletion signal. The three panels of Figure 2 show typical data at pH 5.7 (A), pH 7.8 (B), and pH 9.5 (C). For clarity, the traces at 500 nm (which are similar to those at 490 nm) are not displayed. At each pH value, the four time traces were fitted simultaneously starting 20 μs after the flash. Three exponentials were required to fit the data adequately at each pH. These fits (dotted lines) are also shown in Figure 2. They are clearly satisfactory, except for the early time region, which we excluded, and which is irrelevant for our purposes. From Figure 2A, we conclude that at pH 5.7 the I_1/I_2 equilibrium is almost completely on the side of I_2/I_2', since the signal amplitude at 490 nm is negative after the rise of I_2 (ground-state depletion dominates the I_1 contribution). From the fit, we obtained a time constant of 850 μs for the I_1 to I_2 transition, and of 18 ms for the I_2 to I_2' transition. The assignment of the latter time constant to I_2 to I_2' transition is not obvious from the data of Figure 2 but will be clarified on the basis of the corresponding amplitude spectrum discussed below. The recovery of P is extremely slow at this pH with a time constant of 30 s. Thus, the complete return of the absorbance changes to the baseline could not be recorded with our time base ending at 50 s.

Examination of the time traces at pH 7.8 for Y98Q (Figure 2B) indicates that profound changes occurred between pH 5.7 and 7.8. The 500 and 490 nm traces, indicative of the I_1 population, now no longer decay to zero at the rise of I_2 but retain a large positive amplitude, finally decaying to zero together with I_2'. At this pH, the I_1/I_2 equilibrium has shifted to I_1 as compared to pH 5.7. In agreement with this, we observe that the amplitude of the trace at 350 nm, indicative of the I_2/I_2' population, clearly decreased relative to the initial I_1 amplitude (comparing panels A and B of Figure 2). This same effect may also be observed in the depletion signal at 450 nm, where the amplitude of the absorbance decrease around 1 ms associated with the I_1 to I_2/I_2' transition is smaller at pH 7.8 (Figure 2B) than at pH 5.7 (Figure 2A). We note that all three time constants are significantly accelerated at pH 7.8 relative to pH 5.7: τ_1 is now 480 μs, τ_2 is 2.5 ms, and τ_3 is 9.5 s.

The time traces in Figure 2C show that, between pH 7.8 and 9.5, further changes occur in the opposite direction. The positive amplitude of the 500 and 490 nm traces remaining after the rise of I_2 and I_2' in the time range between 1 ms and 1 s is reduced, suggesting that less I_1 is in equilibrium with I_2/I_2' than at pH 7.8. At the same time, however, the amplitude of the 350 nm time trace, measuring the I_2/I_2' amplitude, has also decreased. This may be concluded from a comparison of the ratios of the 350 nm amplitude to the initial amplitudes at 490 and 500 nm and from the smaller increase in the depletion signal around 1 ms at pH 9.5. The three time constants all increased between pH 7.8 and 9.5: τ_1 is now 780 μs, τ_2 is 7.4 ms, and τ_3 is 20 s. We note that the initial amplitudes at 490 and 500 nm as well as the initial depletion signal remained approximately constant with pH. This suggests that the amount of I_1 generated by the flash is almost pH independent.

These measurements were repeated at 15 pH values between pH 5.7 and 10.1 and analyzed as described. The three rate constants ($k_i = \tau_i^{-1}$) from the fits are plotted in Figure 3 against pH. They display bell-shaped dependencies as suggested by the data of Figure 2. Between pH 5.7 and 8, all three rates increase by factors between 2 (k_1) and 8 (k_2). This is in contrast to wild type (*40*), where k_1 slows from pH 5 to 8. The overall cycle (k_3) is fastest around pH 8 similar to wild type and has the same bell-shaped curve as wild type (*40*). Above pH 8, all three rate constants decrease again.

Amplitudes are more appropriate measures to determine the pK_a values than rates. To quantify the pH dependence of the I_1/I_2 equilibrium, the amplitude A_3 of the third and slowest component at each of the four wavelengths was normalized to the initial absorbance change (initial bleach): $A_3/\Sigma_i A_i$. Since, at 350 nm, the initial amplitude is close to zero (Figure 2), it was normalized to the initial absorbance change at 490 nm, which as noted above is to a good

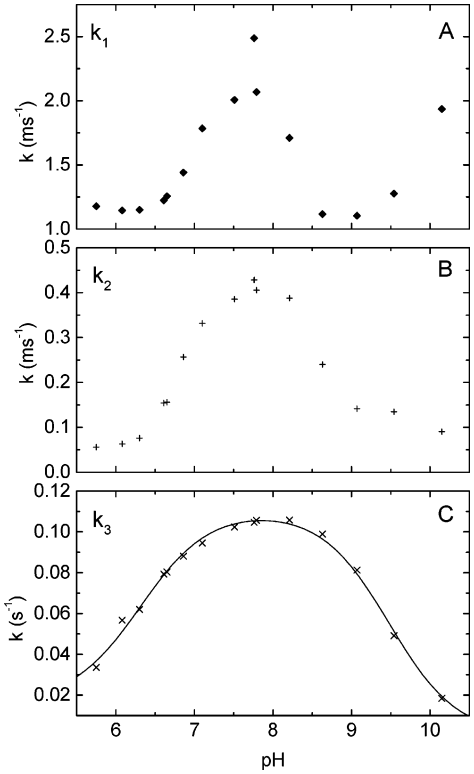

FIGURE 3: Y98Q rate constants determined from simultaneous fits to the transient absorption time traces at 450, 350, 490, and 500 nm (see Figure 2) at 15 pH values ranging from pH 5.75 to pH 10.15. (A) First, (B) second, and (C) third exponential relaxation component. The solid curve in (C) is a fit according to a model described in the text with pK_a's of 6.3 and 9.5.

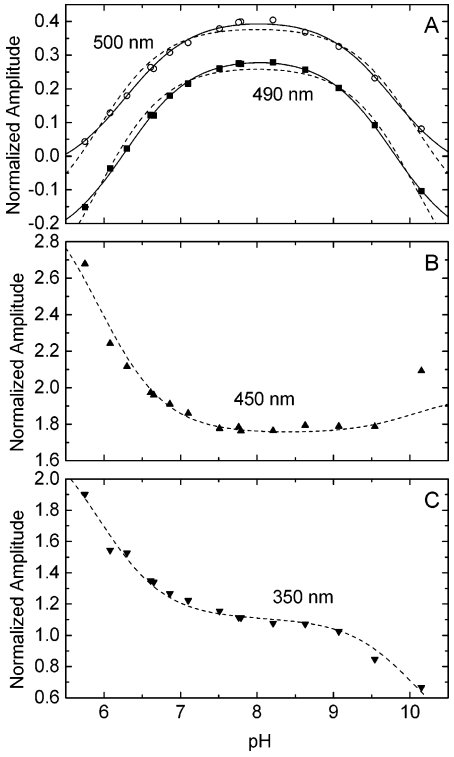

FIGURE 4: Normalized amplitudes of the third exponential relaxation component determined from simultaneous fits to the traces at 450, 350, 490, and 500 nm (see Figure 2) at 15 pH values ranging from pH 5.75 to pH 10.15. (A) 490 and 500 nm, (B) 450 nm, (C) 350 nm. The normalization at 450, 490, and 500 nm refers to the extrapolated initial absorbance change, i.e., the sum of the three amplitudes at the respective wavelengths. The A_3 amplitude at 350 nm (panel C) was normalized to the extrapolated initial absorbance change at 490 nm. The solid lines in (A) are simultaneous Henderson−Hasselbalch fits to the data at 490 and 500 nm only, resulting in pK_a's of 6.3 and 9.8. The dashed lines in panel A−C represent simultaneous fits to the data at all four wavelengths with pK_a's of 5.9 and 10.1.

approximation pH independent. The corresponding normalized amplitudes are plotted against pH in Figure 4. At 490 and 500 nm (Figure 4A), these amplitudes (measuring the relative amount of I_1 remaining after the I_1 to I_2/I_2' transitions, i.e., after establishment of the $I_1/I_2/I_2'$ equilibrium) show the expected increase with pH from pH 5.7 to 8. The amplitude at 350 nm (Figure 4C), a measure of I_2/I_2', shows the corresponding decrease in this pH interval. Together, these observations provide further evidence that, in this pH range, an increase in pH shifts the I_1/I_2 equilibrium in the direction of I_1. This is confirmed by the pH dependence of the amplitude at 450 nm (Figure 4B). The total amplitude of the depletion signal decreases from pH 5.7 to 8. Since the initial amount of I_1 is pH independent, this means that the amount of I_2/I_2' decreased.

At alkaline pH, above pH 8, an additional effect sets in that is not just the opposite of what occurs at low pH. The normalized I_1 amplitude decreases but there is no corresponding increase at 350 nm. In fact, there is also a decrease at 350 nm. This means that this is not a simple reversal of the I_1/I_2 equilibrium at alkaline pH. Instead, we interpret these observations in terms of an additional equilibrium with an intermediate I_1', which, as we will see below, absorbs around 425 nm. This second equilibrium leads to a decrease in the populations of both I_1 and I_2/I_2' at alkaline pH. With I_1' absorbing between I_1 and I_2, the absorbance at 450 nm would remain approximately constant with pH due to the compensating contributions from I_1 and I_1', as observed (Figure 4B).

To establish the kinetics and spectral properties of this intermediate I_1', the transient absorption changes were measured at pH 10.2 at 20 wavelengths between 330 and 510 nm. From these data, the amplitude spectra were calculated (Figure 9E), which confirmed the contribution of an I_1' intermediate absorbing around 425 nm in equilibrium with I_1 and I_2'. Kinetically, this intermediate is the decay product of I_1. This analysis is discussed in the section on amplitude spectra below to allow a comparison with the amplitude spectra of wild type, Y98F, and Y98Q at pH 7 and 8.

The bell-shaped pH dependencies of the apparent rate constant k_3 and the normalized amplitudes $A_3/\Sigma_i A_i$ for the return of the $I_1/I_1'/I_2$ equilibrium to P were fitted with a model that makes the following assumptions. I_2 is in pH-dependent equilibrium with I_1 which in turn is in equilibrium with I_1', and the microscopic rates for the return from these three states to P are pH-independent. The fit to k_3 then resulted in pK_a values of 6.3 and 9.5 (Figure 3C). A simultaneous fit of the amplitude data at 490 and 500 nm led to an excellent fit with pK_a values of 6.3 and 9.8 (solid lines Figure 4A). From a simultaneous fit of the amplitude data at all four wavelengths, pK_a values of 5.9 and 10.1 were obtained (dashed lines in Figure 4A−C), although this fit was not as good as that of the simultaneous fit of just the 490 and 500 nm amplitudes. In summary, the pK_a for the I_1/I_2 equilibrium is ~6.2, and the pK_a for the I_1/I_1' equilibrium is ~10.

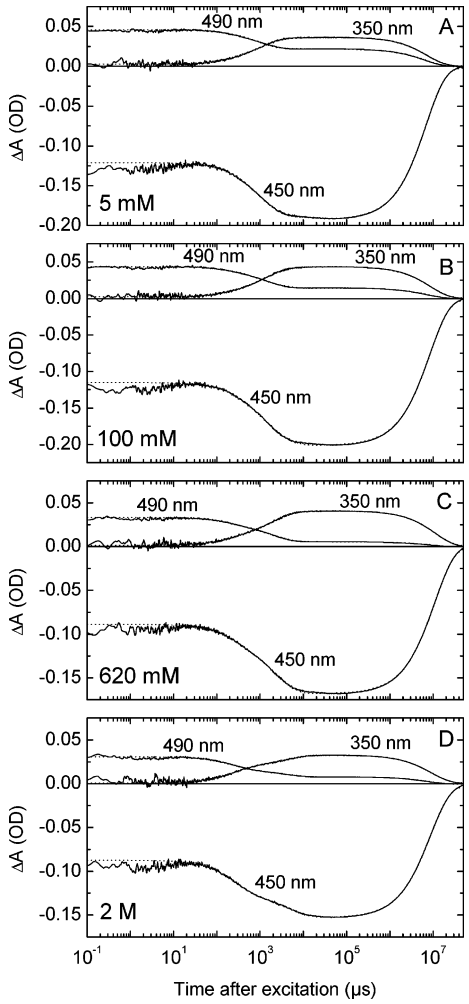

FIGURE 5: Transient absorption changes of the mutant Y98Q after laser flash excitation at 430 nm measured at the three wavelengths 450, 350, and 490 nm, as indicated, at increasing concentrations of KCl. (A) 5 mM, (B) 100 mM, (C) 620 mM, (D) 2 M. The traces are averages of 20 scans. Conditions: 50 mM Tris buffer, pH8.0, 20 °C. The dotted lines are simultaneous fits to the traces at 450, 350, 490, and 500 nm (data not shown) with three exponentials in the time range from 20 μs to 50 s.

Salt Dependence. The photocycle kinetics of Y98Q were measured at the four wavelengths 350, 450, 490, and 500 nm at pH 8 in 50 mM Tris buffer and KCl concentrations between 0 and 2 M. The pH was chosen where the photocycle recovery is fastest (see Figure 3C). Figure 5 shows typical data at selected KCl concentrations. The traces at 500 nm are similar to those at 490 nm and are not shown for clarity. At KCl concentrations below 10 mM, the data demonstrate that the I_1/I_2 equilibrium is on the side of I_1 (panel A, trace at 490 nm) and that the kinetics are not significantly affected by the salt concentration. Starting at 20 mM KCl, the I_1 equilibrium amplitude remaining in the 10 ms to 1 s time range, as monitored by the absorbance change at 490 and 500 nm, decreases, and simultaneously the I_2/I_2' amplitude in this time range, as monitored by the absorbance change at 350 nm, increases. This may be concluded from a comparison of the time traces in Figure 5 at 5 mM (panel A) and 100 mM (panel B) KCl. The initial amount of I_1 at 100 ns, as indicated by the 490 nm trace, is the same under these salt conditions. The amount of I_1 remaining after the formation of I_2' is clearly less at 100 mM than at 5 mM. At the same time, the amount of I_2/I_2' estimated from the 350 nm trace is higher at 100 mM. This is supported by the fact that the absorbance change in the depletion signal (450 nm) around 1 ms due to the I_1 to I_2/I_2' transition is larger at 100 mM. At 620 mM KCl (Figure 5C), even less I_1 remains in the millisecond time range and the amount of I_2/I_2' is maximal. The traces at 2 M KCl (Figure 5D) show that, at this very high ionic strength, the trend is reversed and that a qualitative change occurs in the kinetics involving the amplitude and kinetics of the I_2 to I_2' transition. Under these conditions, the I_1 to I_2 and I_2 to I_2' transitions can be clearly discerned as separate phases in the time traces (Figure 5D). At each salt concentration, a simultaneous fit to the data at the four wavelengths required three exponentials. The corresponding three rate constants are plotted against the log of the KCl concentration in Figure 6. These data show that k_1 and k_2, for the I_1 to I_2 and I_2 to I_2' transitions respectively, are increased 3−4-fold by salt, reaching typical wild type values around 600 mM KCl. The rate constant of the ground-state recovery, k_3, shows opposite behavior and is slowed up to about 600 mM KCl (Figure 6C). The solid line is a fit to the data and will be explained below. Above this concentration, the effect is reversed and the cycle is accelerated. Over the whole salt range, the time constant of ground-state recovery of Y98Q remains between 7 and 12 s, which is 30−60 times slower than in wild type. As with the pH measurements, the normalized amplitude of the third component, A_3, is an appropriate measure of the I_1/I_2 equilibrium (Figure 7). The normalized data at 500 and 490 nm (Figure 7A) provide the best measure of the relative amounts of I_1, since the signals at these wavelengths are

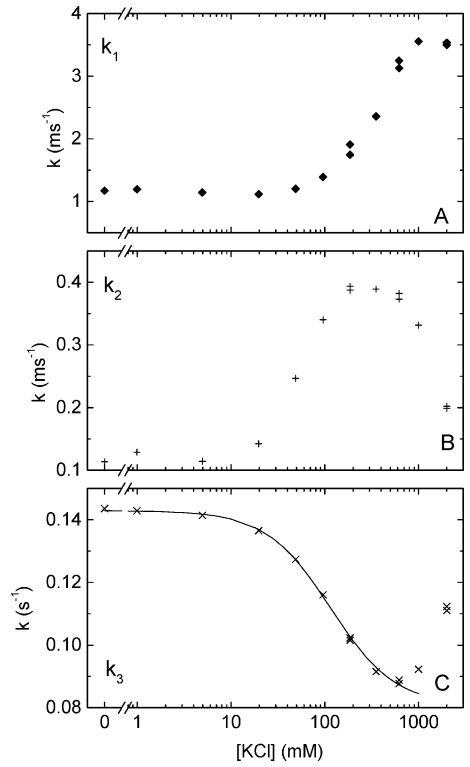

FIGURE 6: Rate constants determined from simultaneous fits to the traces at 450, 350, 490, and 500 nm (see Figure 5) at 14 concentrations of KCl ranging from 0 to 2 M. (A) First, (B) second, and (C) third exponential relaxation component. The fit in C used eq 2 with the same parameters as for the equilibrium binding curves of Figure 7.

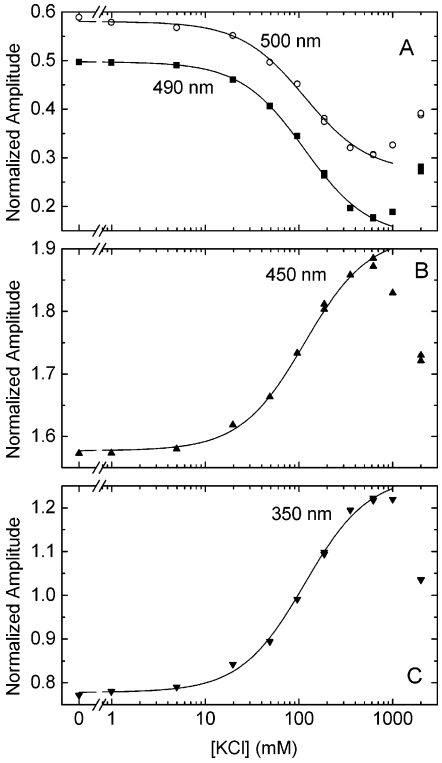

FIGURE 7: Normalized amplitudes of the third exponential relaxation component determined from simultaneous fits to the traces at 450, 350, 490, and 500 nm (see Figure 2) at 14 concentrations of KCl ranging from 0 to 2 M. (A) 490 and 500 nm, (B) 450 nm, (C) 350 nm. The normalization procedure is the same as for Figure 4. The solid lines are simultaneous fits to the data at the four wavelengths from 0 to 620 mM using eq 2 with $K = 115$ mM and $n = 1.3$.

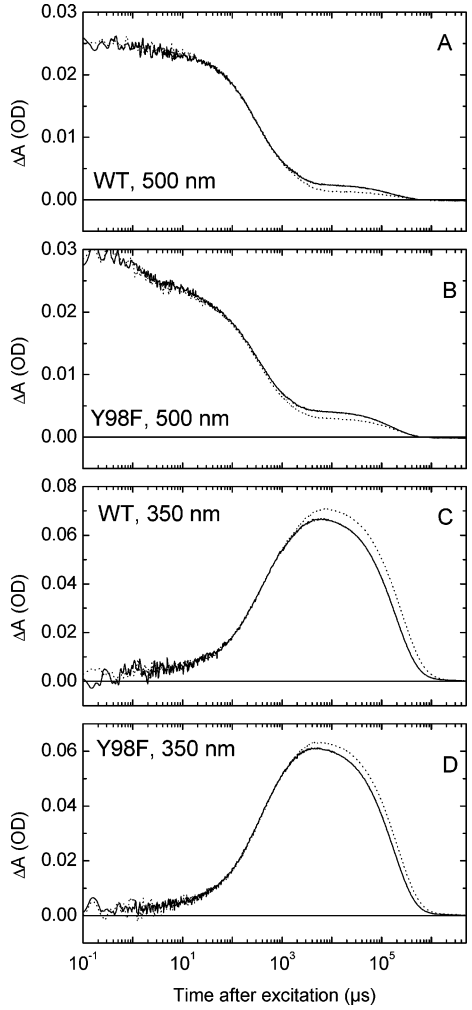

FIGURE 8: Transient absorption changes of PYP WT (A, C) and the mutant Y98F (B, D) after laser flash excitation at 430 nm measured at 500 (A, B) and 350 (C, D) nm without KCl (solid lines) and in 50 mM KCl (dotted lines). The traces are averages of 60 scans. Conditions: 50 mM Tris buffer, pH 7.0, 20 °C.

almost entirely due to I_1. With increasing KCl, the I_1 concentration coexisting with I_2/I_2' decreases until about 600 mM. Above this concentration a reversal sets in. Panels B and C of Figure 7 show the normalized amplitudes at 450 and 350 nm, respectively. The data at 350 nm indicate that the relative concentration of I_2/I_2' increases with salt. The data at 450 nm confirm that the I_2/I_2' contribution in the I_1/I_2 equilibrium increases with salt. At high salt, the effect reverses also at 350 and 450 nm. To separate these two opposing effects, we omitted the high salt data points above 620 mM and fitted the remaining points at all four wavelengths simultaneously with the binding function eq 2, which describes ion binding to I_1 with simultaneous (concerted) conversion to I_2'. The solid lines are the best fit and show that this model with $n = 1.3$ and $K = 115$ mM provides quite a reasonable description of the data below 620 mM. Assuming salt-independent microscopic rates for the return to P from I_1 and I_2/I_2' and rapid equilibration between I_1, I_2, and I_2', the apparent recovery rate k_3 can be fitted to the same model function. Figure 6C shows this fit, using the same parameters as in Figure 7. The fact that the data at all four wavelengths and the recovery rate k_3 can be fitted with the same parameters confirms that the decrease in concentration of I_1 is coupled to a corresponding increase in I_2/I_2'. Possible candidates for the ion binding site that induces the I_1 to I_2' transition will be proposed in the discussion. Approaching 620 mM, the data are distorted by the opposing effect at high salt, and it is thus likely that the true Hill coefficient n is somewhat larger than 1.3 and the true dissociation constant K is smaller than 115 mM. We will interpret these opposing effects in more detail in the discussion. For now, it suffices that we will attribute the effect of KCl above 600 mM to the kosmotropic properties of this salt leading to stabilization of the compact and folded I_1 structure.

The salt-induced shift in the equilibrium from I_1 to I_2' is not limited to Y98Q. It is easiest to observe in this mutant because the ratio of the I_1 and I_2/I_2' populations is close to 1 at zero salt. Figure 8 shows that increasing KCl from 0 to 50 mM leads to decreases in the absorbance changes at 500 nm and complementary increases at 350 nm, indicating shifts in the equilibria of both wild type and Y98F from I_1 to I_2/I_2'.

Amplitude Spectra and Differential Effect of Salt on I_1/I_2 and I_2/I_2' Equilibria. To learn more about the intermediate spectra in the mutants and to pinpoint the salt effect in the photocycle, the kinetics of wild type, Y98F, and Y98Q were measured at 19 wavelengths from 330 to 510 nm. The data field was subjected to SVD analysis as described. The traces associated with the significant singular values were fitted with a sum of four exponentials for wild type and Y98F from 1 μs to 2 s. From these, the four model-free amplitude spectra

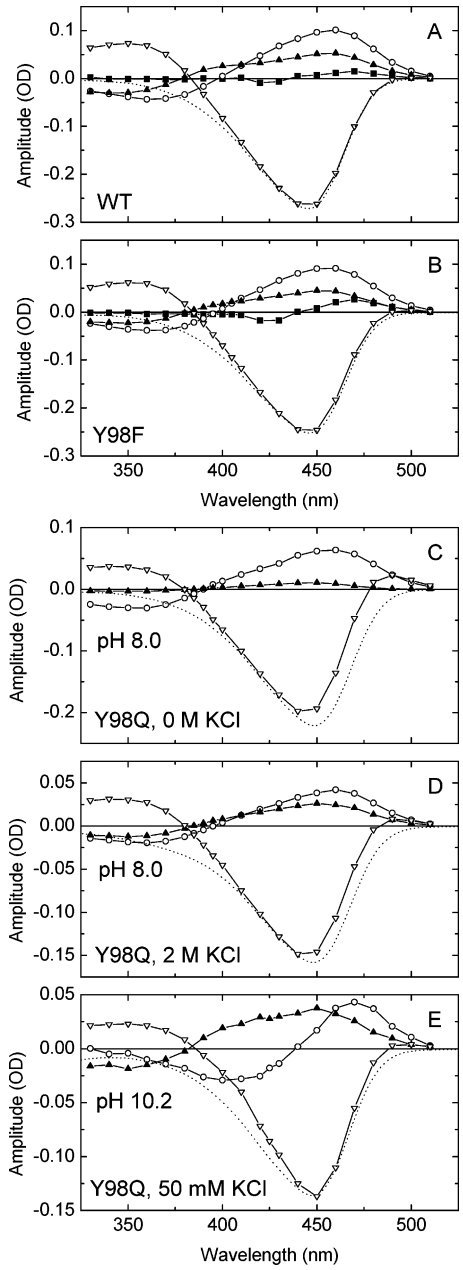

FIGURE 9: Amplitude spectra $B_i(\lambda)$ calculated from the exponential fits to the SVD time traces and the corresponding basis spectra (data not shown). (A) WT, 50 mM Tris, 50 mM KCl, pH 7.0, four relaxation components in the time range from 2 μs to 5 s: $\tau_f = 5.9$ μs (■), $\tau_1 = 280$ μs (○), $\tau_2 = 2.0$ ms (▲), and $\tau_3 = 260$ ms (▽). (B) Y98F, 50 mM Tris, 50 mM KCl, pH 7.0, four relaxation components in the time range from 2 μs to 5 s: $\tau_f = 6.5$ μs (■), $\tau_1 = 290$ μs (○), $\tau_2 = 1.7$ ms (▲), and $\tau_3 = 210$ ms (▽). (C) Y98Q, 50 mM Tris, without KCl, pH 8.0, three relaxation components in the time range from 50 μs to 50 s: $\tau_1 = 860$ μs (○), $\tau_2 = 9.3$ ms (▲), and $\tau_3 = 7.0$ s (▽). (D) Y98Q, 50 mM Tris, 2 M KCl, pH 8.0, three relaxation components in the time range from 50 μs to 50 s: $\tau_1 = 280$ μs (○), $\tau_2 = 5.0$ ms (▲), and $\tau_3 = 8.9$ s (▽). (E) Y98Q, 50 mM Tris, 50 mM KCl, pH 10.2, three relaxation components in the time range from 50 μs to 50 s: $\tau_1 = 500$ μs (○), $\tau_2 = 950$ ms (▲), and $\tau_3 = 27$ s (▽). Dotted lines are scaled and inverted ground-state spectra from steady-state measurements.

$B_i(\lambda)$ were constructed (see eq 1). These are shown for wild type and Y98F in Figure 9, panels A and B, respectively, at pH 7 and 50 mM KCl. Visual inspection shows that these amplitude spectra are virtually identical. This coupled with the similar time constants (these values are collected in Table 1) establishes that the photocycle mechanism and intermediate spectra are the same for these two proteins.

The first transition has a small amplitude and time constant of about 6 μs. This kinetic component was easily recognizable in the time traces at 500 nm in Figure 1 and at other wavelengths. The nature of this transition remains obscure. The second transition at 280−290 μs is the I_1 to I_2 transition. This may be concluded from the positive maximum at 460 nm and the negative minimum near 360 nm (Figure 9A). The third transition at 1.7−2.0 ms is due the I_2 to I_2' conversion. Although no accurate spectra are available for I_2 and I_2', there is evidence that this transition is accompanied by a small blue shift (*29*, *31*). The clear blue shift in the negative minimum of the second amplitude spectrum from about 362 nm (I_2) to around 350 nm (I_2') in the third amplitude spectrum is in agreement with this interpretation (see Figure 9A). The positive maximum at 460 nm is due to I_1 and shows up in the I_2 to I_2' amplitude spectrum since I_1 is coupled to I_2 via the equilibrium. The positive shoulder near 400 nm is probably due to I_2. The fourth transition at 210−260 ms is the recovery of P.

Also shown in Figure 9 is an inverted spectrum of P (dotted line), scaled to best fit the amplitude spectrum for the I_2' to P transition above 420 nm. The fit is almost perfect for wild type (Figure 9A), suggesting that the contribution from other intermediates besides P is very small in this wavelength range. For Y98F, the corresponding fit is not quite as good, with small systematic deviations occurring above 460 nm with the greatest difference around 490 nm (Figure 9B). This indicates a small contribution from I_1 in the decay to P and is of course in agreement with the 500 nm time traces for this mutant in Figures 1C and 8B, which suggest that the I_1/I_2 equilibrium is more on the I_1 side than in wild type.

The corresponding results for Y98Q at pH 8, at which the photocycle is fastest, are shown in Figure 9C,D for two ionic strengths. This pH was chosen to make data collection at multiple wavelengths feasible, but some data were also collected at pH 7 (see below). For Y98Q, the SVD analysis required only two significant singular values for the time interval from 50 μs to 50 s, suggesting that only two spectral species (I_1 and I_2/I_2') contribute at this pH. The time traces associated with the two significant singular values were fitted with a sum of three exponentials. The early microsecond component is absent because it was excluded by the time range used. At zero KCl, the three time constants are 860 μs, 9.3 ms, and 7.0 s (these numbers differ from those in Table 1, which refer to 50 mM KCl; see also Figure 6). The corresponding amplitude spectra are shown in Figure 9C. The first transition is I_1 to I_2, with its amplitude spectrum strongly resembling that for the corresponding transition in wild type (Figure 9A). The second transition at 9.3 ms is due to the I_2 to I_2' transition. Its amplitude spectrum has a much smaller magnitude than in wild type and Y98F in particular in the near UV where a negative contribution due to the formation of I_2' would be expected. This suggests that this transition, the conformational change, is significantly inhibited, if not absent, at low salt.

The third Y98Q amplitude spectrum, for the final decay to P (7.0 s), differs strongly from that for wild type. Positive absorbance at 350 nm (I_2) and 490 nm (I_1) now decay together to P. The amplitude spectrum above 420 nm cannot

be fitted with a scaled P spectrum, as there are large deviations due to a contribution from I_1. The third amplitude spectrum provides additional strong evidence for an I_1/I_2 equilibrium, with I_1 decaying together with I_2 to P.

Figure 9D shows the amplitude spectra for Y98Q at 2 M KCl. SVD analysis again reveals only two spectrally distinguishable species. Fitting the two singular value time traces with three exponentials yields time constants of 280 μs, 5 ms, and 8.9 s. At high salt, the first two time constants are faster, and the third is slower than at zero salt. The most striking difference between the two sets of amplitude spectra in panels C and D is that the relative magnitude of the I_2 to I_2' transition (second amplitude spectrum) is much larger at 2 M KCl. This suggests that salt facilitates the I_2 to I_2' transition. At high salt, there is not only less I_1 and more I_2 and I_2', but the fraction of molecules in I_2' is much increased. A major effect of salt thus appears to be on the structural transition between I_2 and I_2'. We also determined the amplitude spectra at pH 7 at 0 and 50 mM KCl but at fewer wavelengths (data not shown). Qualitatively similar results were obtained. Importantly, these amplitude spectra clearly showed that the salt-induced increase in the amplitude of the I_2 to I_2' transition occurred already in the 0 to 50 mM KCl range at pH 7. Thus, this salt effect on the I_2 to I_2' amplitude apparently occurs in the same concentration range as the ion binding that we discussed above.

The wavelength dependence of the transient absorption changes of Y98Q was measured at pH 10.2 (50 mM KCl, Tris buffer) to determine the intermediate spectra at alkaline pH. In contrast to the results at pH 8.0, three singular values were required at this pH, suggesting the presence of three spectrally distinguishable species (I_1, I_1', and I_2/I_2'). The singular value traces were fitted with three exponentials with time constants of 500 μs, 950 μs, and 27 s. The corresponding amplitude spectra were constructed according to ref *38* and are presented in Figure 9E. There is a striking difference with the results at pH 8.0. The first transition is now from I_1 to I_1', which clearly absorbs above 400 nm. Further analysis using a matrix method to determine the intermediate spectra of chromoproteins from their transient absorption changes in a model-independent way (*37*) indicates that the absorption maximum is around 425 nm. The only assumption of this procedure is that the absorbance of I_2/I_2' is zero above some wavelength (we used 430 nm). The second amplitude spectrum, in Figure 9E, suggests that, in this transition an equilibrium of I_1 and I_1' decays to I_2'. The amplitude spectrum of the final transition implies that an equilibrium of I_2', I_1, and I_1' decays to P. The data clearly indicate that I_1' is kinetically between I_1 and I_2'. We suggest that I_1' has the structure of I_2' with a surface-exposed chromophore (*28*), which is deprotonated at this pH.

Using the same matrix method (*37*), we calculated the spectra of I_1, I_2/I_2', and P for Y98Q at pH 8 at 0 and 2 M KCl from the flash data. These spectra are shown in Figure 10. The I_1 and I_2/I_2' spectra depend only very weakly on this choice. The wild type spectra were constructed in the same way. There are no significant differences between the spectra in Y98Q and wild type. The fact that only two major spectral species are found implies that the I_1 in equilibrium with I_2 is spectrally identical to I_1 formed initially.

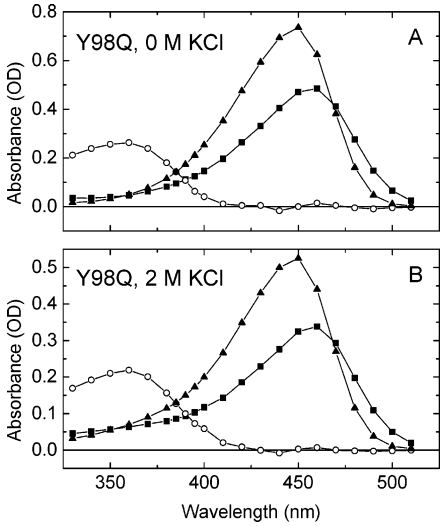

FIGURE 10: Intermediate spectra, I_1 (■) and I_2 (○), calculated from the amplitude spectra of Figure 9C,D and the ground-state spectrum (▲) from a steady-state measurement. Unique intermediate spectra were obtained by using the constraint that I_2 does not contribute to absorption for $\lambda \geq 430$ nm. (A) Y98Q, 50 mM Tris, without KCl, pH 8.0. (B) Y98Q, 50 mM Tris, 2 M KCl, pH 8.0.

DISCUSSION

The photocycle of the mutant Y98Q differs in a number of significant ways from that of wild type PYP. The decay of I_2' is slowed dramatically, there is a moderate slowing in the rise of I_2 and I_2', the I_1/I_2 equilibrium is strongly shifted toward I_1 at pH 8, and finally, there is a large pH and salt effect on this equilibrium. In contrast, the photocycle of Y98F is virtually unaffected as compared to wild type. Y98 is conserved in five out of seven known PYP species. In the two where it is not conserved, it is replaced by F, another residue with an aromatic ring. These results suggest the requirement for an aromatic ring structure at this position. The high-resolution NMR structure of the dark state of PYP in solution provides a partial explanation for this apparent requirement (*32*). The NMR studies exclude a hydrogen bond between R52 and the carbonyl of Y98, as observed in the crystal structure (*9*). Instead, they provide evidence for a cation$-\pi$ interaction between the guanidinium group of R52 and the aromatic ring of Y98 (*32*). Such interactions are known to contribute as much to protein stability as a hydrogen bond (*41*). In PYP, the $\alpha_3-\alpha_4$ loop may be linked with the $\beta_4-\beta_5$ loop via this R52−Y98 interaction in the dark state P. The Y to F replacement would not significantly alter this stabilizing interaction. In the Y to Q mutation, on the other hand, this interaction would be lost, leading to a more flexible conformation of the $\beta_4-\beta_5$ loop. A number of residues in this loop are part of the chromophore binding pocket. Prominent among these is M100, the mutation of which leads to dramatic changes in the photocycle kinetics, in particular a 1000-fold slower decay of I_2' in the M100A mutant (*33*).

The crystal structure of the PYP domain of Ppr, in which Y98 is naturally replaced by F, has been solved (*42*). It has a structure for the $\beta_4-\beta_5$ loop that is very different from *H. halophilia* PYP. In Ppr, M100 is removed from the direct chromophore environment. There is no evidence however for an interaction between the side chain of R52 and the aromatic ring (*42*). In fact, the position of F98 of Ppr differs

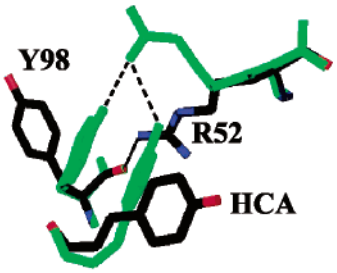

FIGURE 11: Molecular modeling of Y98, R52, and the PYP chromophore (HCA) in the dark state (black) and in I_2' (green). In the dark structure, based on PDB 2PYP (*10*), there is a hydrogen bond between R52 and the carbonyl of Y98. In the I_2' intermediate, the structures of R52 and the isomerized chromophore are based on PDB 2PYP (*10*). The geometry of Y98 was obtained using the torsion function of Deep View (Swiss Pro) to rotate the side chain followed by energy minimization to avoid bad contacts. The planes of the ring systems of Y98 and the chromophore are approximately 2.9 Å apart.

significantly from that of Y98 in *H. halophilia* PYP, where it is on the surface and pointing outward. In Ppr, it is much closer to the chromophore. The dark state structure of the PYP domain of Ppr was characterized as "I_2-like" (*42*), and this conformation might be induced (stabilized) by the proximity of the F98 ring to the chromophore.

A related structural clue for the effect of Y98Q may thus be found in the transient structures of the intermediates. After isomerization and rotation out of the binding pocket, the chromophore ring may interact with the ring of Y98 or F98, thereby stabilizing the I_2 structure through a $\pi-\pi$ stacking interaction. In the absence of a ring, such as in Y98Q, the I_1/I_2 equilibrium may be more on the side of I_1 because of the lack of a stabilizing interaction in I_2. Using molecular modeling, we found that, with reasonable dihydral angles for the Y98 side chain, such an interaction would be possible. Figure 11 compares the dark state P and the I_2 state, with the tyrosine 98 rotated about the C_α side chain bonds. Note the stacking of the aromatic ring systems (chromophore and Y98) and the postulated hydrogen bonds between the guanidinium group of R52 and the tyrosine hydroxyl as well as the chromophore. Recently, evidence was presented for a transient stacking interaction between the flavin chromophore and a nearby tyrosine in the blue-light receptor AppA (*43*).

Effect of pH. In previous work, we demonstrated the presence of a pH-dependent I_1/I_2 equilibrium in wild type at alkaline pH (*28*) and in the mutants E46Q and E46A at pH 7 (*28*). At high pH, these equilibria shifted toward I_1. Similar observations have been made for wild type (*29*) and were subsequently confirmed by other workers (*30*). Here, we present evidence that a pH-dependent equilibrium is also present in the mutant Y98Q with a pK_a of about 6.3. This pK_a is much lower than that of wild type, where values above 11 (*28*) and of 10 (*30*) were obtained and also lower than in E46Q (pK_a $\sim$ 8.1) and E46A (pK_a $\sim$ 8.8) (*28*). For the interpretation of these equilibria in E46Q and E46A, we introduced an additional intermediate I_1' between I_1 and I_2, which seemed to be spectrally indistinguishable from I_1 (*28*). In this proposal, we hypothesized that in I_1', the deprotonated chromophore has swung out of the binding pocket toward the surface, where it picks up a proton to form I_2. The pK_a values for E46Q and E46A characterize the I_1'/I_2 equilibrium of the exposed chromophore at the surface. This pK_a might be lowered in Y98Q, if the chromophore is less exposed in I_1' and I_2. Up to pH 8, the three rate constants for I_1/I_2, I_2/I_2', and I_2'/P all increased with pH (Figure 3). An acceleration with pH was also observed with the E46Q and E46A mutants (*28*). Between pH 5.7 and 8.0, the I_1/I_2 equilibrium in Y98Q shifts in the direction of I_1 (Figure 4A,C).

Above pH 8, however, the pH dependence of the rate constants reverses (Figure 3), and the relative amounts of I_1 and I_2 decrease (Figure 4A,C) with a pK_a of about 9.8. These observations suggested that at alkaline pH, I_1 and I_2' are in equilibrium with an additional species absorbing between 400 and 450 nm (Figure 9E). This could explain the approximate pH independence of the normalized amplitude at 450 nm (Figure 4B). Convincing kinetic and spectral evidence for the existence of this intermediate was obtained from analysis of the amplitude spectra at pH 10.2, indicating maximal absorbance around 425 nm (Figure 9E). On the basis of its λ_{max} value, we expect that this intermediate has a deprotonated chromophore. We will call this intermediate I_1' because it has a deprotonated chromophore and is the decay product of I_1. It only occurs at alkaline pH. Since I_1' was already introduced for the E46Q mutant, we should rename it there. From the amplitude spectra of Figure 9E, we concluded that the time sequence of the intermediates is I_1, I_1', and I_2', with the I_1/I_1' equilibrium partially decaying to I_2', and finally the $I_1/I_1'/I_2'$ equilibrium decaying to P. I_1' may be considered as a form of I_2' with deprotonated chromophore, the alkaline form of I_2'. Similar results were obtained from analysis of the amplitude spectra of wild type at pH 10 (data not shown; Joshi et al., to be published), suggesting a similar role for I_1'. For wild type, an intermediate absorbing near 410−420 nm at alkaline pH had been proposed previously (*30*, *44*, *29*) and was called PYP_M^{410} (*30*) or pB^{deprot} (*29*). In contrast to the steady-state measurements of refs *30* and *44*, our kinetic data can resolve the rise times of I_1' and I_2' and assign a temporal position for the I_1' intermediate between I_1 and I_2'. In (*29*) pB^{deprot} was introduced between pB (I_2/I_2') and pG (P), with a λ_{max} of $\sim$430 nm, in equilibrium with pB (I_2/I_2') with a pK_a of $\sim$10, and present in the photocycle at any pH. If this intermediate is the same as our I_1', our conclusion that I_1' is the product of I_1 is in disagreement with ref *29*.

Salt/Ionic Lock. The I_1/I_2 equilibrium is present in both wild type and Y98F at pH 7.0 but is far on the side of I_2 with wild type (Figure 8). This equilibrium is also salt-dependent in both systems shifting the equilibrium toward I_2 with increasing salt (Figure 8). In the mutant Y98Q, the equilibrium is much further on the side of I_1 at pH 7.0, and its pH and salt dependence are thus more amenable to characterization.

The KCl concentration had a large effect on the rise and decay times of I_2 and I_2' but most significantly on the I_1/I_2' equilibrium. Figure 6A,B shows that, at low salt, the time constants for the I_1 to I_2 and I_2 to I_2' transitions are slowed by approximately factors of 3−4 in Y98Q with respect to the corresponding wild type values. Around 1 M KCl, these values in Y98Q are close to the wild type values. In this same salt range, the I_1/I_2' equilibrium shifts from predominantly I_1 toward I_2', as in wild type. The salt effect on the kinetics (τ_1 and τ_2 decreasing to facilitate the I_1 to I_2 and I_2 to I_2' conversions) may in part explain the corresponding effect on the I_1/I_2' equilibrium, if we assume that the rates

of the back reactions are not affected by salt. The effect of salt on τ_3, the ground state recovery, is in the opposite direction. Moreover, salt does not bring this decay constant back to its wild type value but slows it down further. Above about 600 mM KCl, the salt effects on the kinetics and equilibria are reversed. This is particularly evident for τ_3 and suggests that two opposing effects are operating with the reversed effect starting to dominate above 600 mM KCl.

The salt dependence of the normalized amplitudes for the I_1/I_2' equilibrium (Figure 7) provides more insight than the rate constants. At all four wavelengths at which the I_1/I_2' equilibrium was monitored, these amplitudes indicate a reversal above 600 mM. Since the normalized amplitudes depend linearly on the fractions of molecules in I_1 and I_2/I_2', respectively, they may be analyzed using a simple binding model (eq 2). This model assumes that KCl binds to an ion pair in I_1 and concomitantly the protein is converted to I_2' in which both the protein structure and the protonation state of the chromophore differ from I_1. The amplitude data at all four wavelengths as well as the recovery rate k_3 could be fitted simultaneously with $n \sim 1.3$ and $K = 115$ mM, if we deleted the highest salt data points (Figure 7). This model is consistent with the PYP crystal structure (*9*), suggesting that a salt linkage between K110 and E12 stabilizes the interaction between the β-scaffold and the N-terminal domain. Ion binding would disrupt this interaction and open the "ionic lock". This model explains why the I_2 to I_2' transition is blocked at low salt. Increasing the salt concentration would shift the equilibrium toward I_2', in which the N-terminal domain is more disordered (*17*), has a different secondary structure (*14*, *19*−*21*), exposes a hydrophobic patch (*15*, *16*, *23*), and presumably detaches from the β-scaffold (*20*, *22*). Importantly, salt binding can thus explain both the acceleration of the I_2 to I_2' transition as well as the slowing of the recovery of P in Y98Q. We note that this ion pair (K/E or K/D) is conserved in all PYP species reported to date, except in Ppr and Ppd, which have a slower and different photocycle (*3*−*5*).

Above 600 mM KCl, the opposing effect dominates and the I_1/I_2' equilibrium is shifted back in the direction of I_1. We believe this reversal which occurs at very high salt is the consequence of the Hofmeister specific ion effect, in which the kosmotropic properties of KCl stabilize the compact folded I_1 structure over the partially unfolded I_2' structure (*45*−*47*).

The amplitude spectra provide further insight into the question at which stage in the photocycle the salt has its major effect. We showed that, in wild type, equilibria exist between I_1 and I_2 (*28*) and between I_2 and I_2' (*31*). In view of our explanation for the shift of the I_1/I_2' equilibrium in terms of the opening of a salt bridge (K110/E12), it seems plausible to assume, as we did in the binding model of eq 2, that, when this salt linkage is broken, the conversion to the structurally altered signaling state I_2' is facilitated. Chromophore protonation (I_2 formation) is known to precede the global conformational change (I_2' formation). It is thus likely that salt has its major effect on the I_2/I_2' equilibrium, thereby also shifting the coupled I_1/I_2 equilibrium. From Figure 9C,D (Y98Q), we conclude that the main difference between the amplitude spectra at 0 and 2 M KCl is that the amplitude of the I_2 to I_2' transition is very small at low salt and comparable to wild type at 2 M salt. Thus, at low salt, the conformational transition I_2 to I_2' is apparently inhibited with the ionic lock is largely intact. Y98Q amplitude spectra at pH 7 show that the magnitude of the I_2 to I_2' transition returns to about half of the wild type value between 0 and 50 mM KCl. This strongly suggests that the salt effect has its major effect on the I_2 to I_2' transition, at relatively low ionic strength, in agreement with the salt binding curves of Figure 7.

Do similar domain interactions as in PYP play a role in the activation of other PAS domain proteins? One of the few PAS domain proteins for which the solution structure of both the resting and the signaling states are known is the LOV2 domain of phototropin (*48*, *49*). Here light-induced distortion of the central β-sheet leads to dissociation of the C-terminal J_α helix from the PAS core and inhibition of the kinase activity (*48*, *49*). This structural change is analogous to the postulated dissociation of the N-terminal domain from the β-scaffold in the activation of PYP.

Salt effects have been previously observed on the rate of the ground-state recovery with wild type (*27*, *50*), but not on the rise time of I_2 and I_2' or on the I_1/I_2' equilibrium. The dependence of the time constant for the ground-state recovery on the NaCl concentration in wild type (*27*), is qualitatively similar to the dependence of τ_3 on the KCl concentration in Y98Q, except for a scaling factor of about 40 in the time constants. The opposing effects between slow of τ_3 at low NaCl and acceleration at high salt were present in wild type as well as in the T6 truncation fragment, in which the first six amino acids from the N-terminal end were removed by enzymatic digestion (*27*). In the T15 fragment, however, in which the first 15 residues were removed, only the high salt acceleration phase remained (*27*). In this fragment, the K110/E12 salt bridge would not exist. These observations are thus consistent with and support our explanation that the low salt phase is due to binding to the K110/E12 ion pair. The authors of ref *27* were the first to call attention to a possible contribution of the K110/E12 salt linkage to the interaction between the β-scaffold and the N-terminal domain.

Salt shifts the conformational equilibrium toward the signaling state I_2' at the relatively low concentration of 100 mM KCl. The activity of PYP may thus be regulated by the intracellular salt concentration, which is on the order of 100 mM.

Integrated pH/Salt Model. The model of eq 2 assumed that the binding of salt induced the transition from I_1 to I_2'. Binding thus leads not only to the conformational change (closed/open) but also to chromophore protonation. The latter implies that the pK_a of the I_1/I_2 equilibrium is significantly higher in the "unlocked/open" structure than in the "locked/closed" structure. An integrated model of both the pH and the salt effects needs to take this pK_a difference into account. We implemented such a model by introducing three states $\{I_2, I_1, I_1'\}$ and $\{\tilde{I}_2, \tilde{I}_1, \tilde{I}_1'\}$ in the closed and open forms, respectively. In each triplet the states are in pH dependent equilibria. The $I_2/\tilde{I}_2$, $I_1/\tilde{I}_1$, and $I_1'/\tilde{I}_1'$ equilibria are moreover salt dependent. This rectangular scheme has thus six species and seven coupled equilibria. Assuming that I_1 and $\tilde{I}_1$ are spectrally indistinguishable, we simulated the fraction of the population in the I_1/I_2 equilibrium that is in I_1 or $\tilde{I}_1$, as well as the effect of salt on this titration curve. Assuming reasonable numbers for the pK_a values and salt binding constants the bell-shaped titration curve of Figure 4A could be reproduced. Identifying $\tilde{I}_2$ with I_2', this model could also

explain the observed shift of the I_1/I_2' equilibrium with increasing salt concentration toward I_2', without significant accumulation of I_2. A qualitatively correct description of both pH and salt dependence of the I_1/I_2' equilibrium was obtained using pK_a's of 6.0 and 8.5 for the I_1/I_2 and $\tilde{I}_1/\tilde{I}_2$ equilibria, respectively, and of 9.5 and 11.5 for I_1/I_1' and $\tilde{I}_1/\tilde{I}_1'$ equilibria, respectively. For more details of this model see Supporting Information. Similar treatments have appeared in the literature before, for example, for the coupled protonation and anion binding in the M_{II} state of rhodopsin (*51*).

Slow Ground-State Recovery. The recovery of P is strongly slowed in Y98Q, by a factor of 40−50 compared to wild type. Since Y98 is located near the chromophore and far away from the K110/E12 salt bridge (on the opposite side of the β-scaffold), it is not obvious how mutation to Q could lead to such a large increase in the I_2' lifetime. The M100A mutation leads to an even greater increase in the time constant for the ground-state recovery (*33*). M100 is the next nearest neighbor of Y98 in the $\beta_4-\beta_5$ loop and likewise close to the chromophore. It is currently believed that the sulfur of M100 catalyzes the reisomerization of the chromophore in the recovery of P (*33*). The Y98Q mutation may thus exert its effect indirectly by altering the conformation of the $\beta_4-\beta_5$ loop and the position of M100 such that it would no longer be able to catalyze recovery. This idea is based on analogy with the PYP from *Rhodospirillum centenum* Ppr, where a significant change in the $\beta_4-\beta_5$ loop structure leads to a repositioning of M100 away from the chromophore (*42*) and a photocycle recovery that is much slower than in PYP from *H. halophila* (*4*). The crystal structure of Y98Q was recently solved and shows indeed that the $\beta_4-\beta_5$ loop and the position of M100 are substantially altered compared to wild type (Savvas et al., to be published).

Rhodopsin Analogy. We showed here for Y98Q and in previous work for wild type (*24*) and the E46Q and E46A mutants (*28*) that the I_1 intermediate is in a pH-dependent equilibrium with the I_2 intermediate and decays together with I_2. Increasing the pH shifts the equilibrium toward I_1. Moreover, we showed that, in Y98Q, Y98F, and wild type, the I_1/I_2 equilibrium is salt-dependent with salt shifting the equilibrium toward I_2' below 600 mM KCl. Both features are reminiscent of the corresponding M_I/M_{II} equilibrium in the activation step of the visual receptor rhodopsin (*52*, *53*). In both photoreceptors, low pH and high salt favor the signaling state, in which a conformational change with surface exposure occurs. The salt dependence of the M_I/M_{II} equilibrium was recently studied in detail (*39*, *53*). It was suggested that an ionic lock involving the conserved motif ERY of helix 3 and E247 of helix 6 holds these helices together in the dark state (*39*). In M_{II}, these helices move apart (*54*, *55*), and this conformational change seems to be a universal feature of G-protein coupled receptors (*56*), which share a common activation mechanism (*57*, *58*). The ionic interaction between these two helices maintains the receptor in the inactive state and has to be broken in the light-induced activation of rhodopsin or in the ligand-induced activation of other G-protein coupled receptors (*57*, *58*). Ion binding also opens this salt linkage, shifting the M_I/M_{II} equilibrium in the direction of the signaling state M_{II} (*39*). Here, we adapted these ideas to PYP by suggesting that the salt linkage K110/E12 stabilizes the interaction between the β-scaffold and the N-terminus in the dark. As in rhodopsin, the I_2 to I_2' equilibrium is associated with a large conformational change and surface exposure in the signaling state I_2'. At very high ionic strength, above 600 mM KCl, salting out of hydrophobic residues is expected to stabilize the compact folded I_2 intermediate over the partially unfolded I_2' state. At high salt, this kosmotropic effect drives the equilibrium back in the direction of I_2 and I_1, as observed.

CONCLUSIONS AND INTERPRETATIONS

(1) Whereas the Y98F mutant had no significant effect on the photocycle kinetics, large effects were observed with the Y98Q mutant. We believe that an amino acid with a conjugated ring system is required at position 98 for a normal photocycle. A ring may help maintain the $\beta_4-\beta_5$ loops with M100 in the proper conformation.

(2) At neutral pH and low ionic strength the I_1/I_2 equilibrium in Y98Q is much further on the side of I_1 than in wild type. This shift in equilibrium in favor of I_1 may be due to the loss of a stabilizing $\pi-\pi$ stacking interaction with the ring system of Y98 in I_2.

(3) With increasing pH the I_1/I_2 equilibrium shifts toward I_1 (p$K_a \sim 6.3$). Beyond pH 8 the populations of I_1 and I_2 decrease and in parallel a new intermediate I_1', absorbing maximally near 425 nm, increases in population (p$K_a \sim 9.8$).

(4) The I_1/I_2 equilibrium shifts toward I_2/I_2' by raising the KCl concentration. This effect is not limited to Y98Q but occurs also in wild type and Y98F.

(5) KCl has two effects on this equilibrium. (i) At low concentration (<20 mM) the formation of the signaling state I_2' is inhibited. Presumably salt binding, with a dissociation constant of 115 mM, leads to the opening of a salt bridge and the concomitant formation of the signaling state I_2'. (ii) Beyond 600 mM KCl the Hofmeister effect dominates and destabilizes the signaling state I_2' by salting out the hydrophobic residues that are exposed in I_2'.

(6) The most likely salt bridge that might be affected at low ionic strength is the ion pair K110/E12 linking the β-scaffold and the N-terminal cap.

ACKNOWLEDGMENT

We thank Elsa Chan and Ingrid Wallat for technical support.

SUPPORTING INFORMATION AVAILABLE

Details of the integrated salt/pH model. This material is available free of charge via the Internet at http://pubs.acs.org.

REFERENCES

1. Meyer, T. E. (1985) Isolation and characterization of soluble cytochromes, ferredoxins and other chromophoric proteins from the halophilic phototrophic bacterium *Ectothiorhodospira halophila*, *Biochim. Biophys. Acta 806*, 175−183.
2. Meyer T. E., Yakali, E., Cusanovich, M. A., and Tollin, G. (1987) Properties of a water-soluble, yellow protein isolated from a halophilic phototrophic bacterium that has photochemical activity analogous to sensory rhodopsin, *Biochemistry 26*, 418−423.
3. Kyndt, J. A., Meyer, T. E., and Cusanovich, M. A. (2004) Photoactive yellow protein, bacteriophytochrome, and sensory rhodopsin in purple phototrophic bacteria, *Photochem. Photobiol. Sci. 3*, 519−530.
4. Jiang, Z. Y., Swem, L. R., Rushing, B. G., Devanathan, S., Tollin, G., and Bauer, C. E. (1999) Bacterial photoreceptor with similarity to photoactive yellow protein and plant phytochromes, *Science 285*, 406−409.

5. Kyndt, J. A., Fitch, J. C., Meyer, T. E., and Cusanovich, M. A. (2005) *Thermochromatium tepidum* photoactive yellow protein/bacteriophytochrome/diguanylate cyclase (Ppd): characterization of the PYP domain, *Biochemistry 44*, 4755−4764.
6. Cusanovich, M. A., and Meyer, T. E. (2003) Photoactive yellow protein: A prototypic PAS domain sensory protein and development of a common signaling mechanism, *Biochemistry 42*, 4759−4770.
7. Taylor, B. L., and Zhulin, I. B. (1999) PAS domains: Internal sensors of oxygen, redox potential, and light, *Microbiol. Mol. Rev. 63*, 479−506.
8. Hellingwerf, K. J., Hendriks, J., and Gensch, T. (2003) Photoactive yellow protein, a new type of photoreceptor protein: Will this "yellow lab" bring us where we want to go? *J. Phys. Chem. A 107*, 1082−1094.
9. Borgstahl, G. E. O., Williams, D. R., and Getzoff, E. D. (1995) 1.4 Angstrom structure of photoactive yellow protein, a cytosolic photoreceptor: unusual fold, active-site, and chromophore, *Biochemistry 34*, 6278−6287.
10. Genick, U. K., Borgstahl, G. E. O., Ng, K., Ren, Z., Pradervand, C., Burke, P. M., Srajer, V., Teng, T. Y., Schildkamp, W., McRee, D. E., Moffat, K., and Getzoff, E. D. (1997) Structure of a protein photocycle intermediate by millisecond time-resolved crystallography, *Science 275*, 1471−1475.
11. Rajagopal, S., Anderson, S., Srajer, V., Schmidt, M., Pahl, R., and Moffat, K. (2005) A structural pathway for signaling in the E46Q mutant of photoactive yellow protein, *Structure 13*, 55−63.
12. Unno, M., Kumauchi, M., Sasaki, J., Tokunaga, F., and Yamauchi, S. (2000) Evidence for a protonated and cis configuration chromophore in the photobleached intermediate of photoactive yellow protein, *J. Am. Chem. Soc. 122*, 4233−4234.
13. Ujj, L., Devanathan, S., Meyer, T. E., Cusanovich, M. A., Tollin, G., and Atkinson, G. H. (1998) New photocycle intermediate in the photoactive yellow protein from *Ectorhodospira halophila:* picosecond transient absorption spectroscopy, *Biophys. J. 75*, 406−412.
14. Xie, A. H., Kelemen, L., Hendriks, J., White, B. J., Hellingwerf, K. J., and Hoff, W. (2001) Formation of a new buried charge drives a large-amplitude protein quake in photoreceptor activation, *Biochemistry 40*, 1510−1517.
15. Borucki, B., Devanathan, S., Otto, H., Cusanovich, M. A., Tollin, G., and Heyn, M. P. (2002) Kinetics of proton uptake and dye binding by photoactive yellow protein in wild type and in the E46Q and E46A mutants, *Biochemistry 41*, 10026−10037.
16. Meyer, T. E., Tollin, G., Hazzard, J. H., and Cusanovich, M. A. (1989) Photoactive yellow protein from the purple phototrophic bacterium, *Ectothiorhodospira halophila*−quantum yield of photobleaching and effects of temperature, alcohols, glycerol, and sucrose on kinetics of photobleaching and recovery, *Biophys. J. 56*, 559−564.
17. Rubinstenn, G., Vuister, G. W., Mulder, F. A. A., Dux, P. E., Boelens, R., Hellingwerf, K. J., and Kaptein, R. (1998) Structural and dynamic changes of photoactive yellow protein during its photocycle in solution, *Nat. Struct. Biol. 5*, 568−570.
18. Craven, C. J., Derix, N. M., Hendriks, J., Boelens, R., Hellingwerf, K. J., and Kaptein, R. (2000) Probing the nature of the blue-shifted intermediate of photoactive yellow protein in solution by NMR: hydrogen−deuterium exchange data and pH studies, *Biochemistry 39*, 14392−14399.
19. Brudler, R., Rammelsberg, R., Woo, T. T., Getzoff, E. D., and Gerwert, K. (2001) Structure of the I1 early intermediate of photoactive yellow protein by FTIR spectroscopy, *Nat. Struct. Biol. 8*, 265−270.
20. Sasaki, J., Kumauchi, M., Hamada, N., Oka, T., and Tokunaga, F. (2002) Light-induced unfolding of photoactive yellow protein mutant M100L, *Biochemistry 41*, 1915−1922.
21. Lee, B.-C., Croonquist, P. A., Sosnick, T. R., and Hoff, W. D. (2001) PAS domain receptor photoactive yellow protein is converted to a molten globule state upon activation, *J. Biol. Chem. 276*, 20821−20823.
22. Imamoto, Y., Kamikubo, H., Harigai, M., Shimizu, N., and Kataoka, M. (2002) Light-induced global conformational change of photoactive yellow protein in solution, *Biochemistry 41*, 13595−13601.
23. Hendriks, J., Gensch, T., Hviid, L., van der Horst, M. A., Hellingwerf, K. J., and van Thor, J. J. (2002) Transient exposure of hydrophobic surface in the photoactive yellow protein monitored with Nile red, *Biophys. J. 82*, 1632−1643.
24. Kelemen, L., Nie, B., Phillip, A., Hoff, W., and Xie, A. (2005) Impact of crystallization on protein structural dynamics, *Biophys. J. 88*, 208a.
25. Vogel, R., Ruprecht, J., Villa, C., Mielke, T., Schertler, G. F. X., and Siebert, F. (2004) Rhodopsin photoproducts in 2D crystals, *J. Mol. Biol. 338*, 597−609.
26. Hoff, W. D., Xie, A., Van Stokkum, I. H. M., Tang, X., Gural, J., Kroon, A. R., and Hellingwerf, K. J. (1999) Global conformational changes upon receptor stimulation in photoactive yellow protein, *Biochemistry 38*, 1009−1017.
27. Harigai, M., Imamoto, Y., Kamikubo, H., Yamazaki, Y., and Kataoka, M. (2003) Role of an N-terminal loop in the secondary structural change of photoactive yellow protein, *Biochemistry 42*, 13893−13900.
28. Borucki, B., Otto, H., Joshi, C. P., Gasperi, C., Cusanovich, M. A., Devanathan, S., Tollin, G., and Heyn, M. P. (2003) pH dependence of the photocycle kinetics of the E46Q mutant of photoactive yellow protein: Protonation equilibrium between I_1 and I_2 intermediates, chromophore deprotonation by hydroxyl uptake, and protonation relaxation of the dark state, *Biochemistry 42*, 8780−8790.
29. Hendriks, J., van Stokkum, I. H. M., and Hellingwerf, K. J. (2003) Deuterium isotope effects in the photocycle transitions of the photoactive yellow protein, *Biophys. J. 84*, 1180−1191.
30. Imamoto, Y., Harigai, M., and Kataoka, M. (2004) Direct observation of the pH-dependent equilibrium between L-like and M intermediates of photoactive yellow protein, *FEBS Lett. 577*, 75−80.
31. Joshi, C. P., Borucki, B., Otto, H., Meyer, T. E., Cusanovich, M. A., and Heyn, M. P. (2005) Photoreversal kinetics of the I_1 and I_2 intermediates in the photocycle of photoactive yellow protein by double flash experiments with variable time delay, *Biochemistry 44*, 656−665.
32. Dux, P., Rubinstenn, G., Vuister, G. W., Boelens, R., Mulder, F. A. A., Hard, K., Hoff, W. D., Kroon, A. R., Crielaard, W., Hellingwerf, K. J., and Kaptein, R. (1998) Solution structure and backbone dynamics of the photoactive yellow protein, *Biochemistry 37*, 12689−12699.
33. Devanathan, S., Genick, U. K., Canestrelli, I. L., Meyer, T. E., Cusanovich, M. A., Getzoff, E. D., and Tollin, G. (1998) New insights into the photocycle of *Ectothiorhodospira halophila* photoactive yellow protein: Photorecovery of the long-lived photobleached intermediate in the Met100Ala mutant, *Biochemistry 37*, 11563−11568.
34. Getzoff, E. D., Gutwin, K. N., and Genick, U.K. (2003) Anticipatory active-site motions and chromophore distortion prime photoreceptor PYP for light activation, *Nat. Struct. Biol. 10*, 663−668.
35. Kyndt, J. A., Vanrobaeys, F., Fitch, J. C., Devreese, B. V., Meyer, T. E., Cusanovich, M. A., and Van Beeumen, J. J. (2003) Heterologous production of *Halorhodospira halophila* holophotoactive yellow protein through tandem expression of the postulated biosynthetic genes, *Biochemistry 42*, 965−970.
36. Kyndt, J. A., Hurley, J. K., Devreese, B., Meyer, T. E., Cusanovich, M. A., Tollin, G., and Van Beeumen, J. J. (2004) *Rhodobacter capsulatus* photoactive yellow protein: Genetic context, spectral and kinetics characterization, and mutagenesis, *Biochemistry 43*, 1809−1820.
37. Borucki, B., Otto, H., and Heyn, M. P. (1999) Reorientation of the retinylidene chromophore in the K, L, and M intermediates of bacteriorhodopsin from time-resolved linear dichroism: resolving kinetically and spectrally overlapping intermediates of chromoproteins, *J. Phys. Chem B 103*, 6371−6383.
38. Borucki, B., Otto, H., Rottwinkel, G., Hughes, J., Heyn, M. P., and Lamparter, T. (2003) Mechanism of Cph1 phytochrome assembly from stopped-flow kinetics and circular dichroism, *Biochemistry 42*, 13684−13697.
39. Vogel, R., and Siebert, F. (2002) Conformation and stability of α-helical membrane proteins. 1. Influence of salts on conformational equilibria between active and inactive states of rhodopsin, *Biochemistry 41*, 3529−3535.
40. Genick, U. K., Devanathan, S., Meyer, T. E., Canestrelli, I. L., Williams, E., Cusanovich, M. A., Tollin, G., and Getzoff, E. D. (1997) Active site mutants implicate key residues for control of color and light cycle kinetics of photoactive yellow protein, *Biochemistry 36*, 8−14.
41. Scrutton, N. S., and Raine, A. R. C. (1996) Cation-π bonding and amino-aromatic interactions in the biomolecular recognition of substituted ammonium ligands, *Biochem. J. 319*, 1−8.

42. Rajagopal, S., and Moffat, K. (2003) Crystal structure of a photoactive yellow protein from a sensor histidine kinase: Conformational variability and signal transduction, *Proc. Natl. Acad. Sci. U.S.A. 100*, 1649−1654.
43. Kraft, B. J., Masuda, S., Kikuchi, J., Dragnea, V., Tollin, G., Zaleski, J. M., and Bauer, C. E. (2003) Spectroscopic and mutational analysis of the blue-light photoreceptor AppA: A novel photocycle involving flavin stacking with an aromatic amino acid, *Biochemistry 42*, 6726−6734.
44. Hendriks, J., Hoff, W. D., Crielaard, W., and Hellingwerf, K. J. (1999) Protonation deprotonation reactions triggered by photoactivation of photoactive yellow protein from *Ectothiorhodospira halophila*, *J. Biol. Chem. 274*, 17655−17660.
45. Brudler, R., Meyer, T. E., Genick, U. K., Devanathan, S., Woo, T. T., Millar, D. P., Gerwert, K., Cusanovich, M. A., Tollin, G., and Getzoff, E. D. (2000) Coupling of hydrogen bonding to chromophore conformation and function in photoactive yellow protein, *Biochemistry 39*, 13478−13486.
46. Meyer, T. E., Devanathan, S., Woo, T., Getzoff, E. D., Tollin, G., and Cusanovich, M. A. (2003) Site-specific mutations provide new insights into the origin of pH effects and alternative spectral forms in the photoactive yellow protein from *Halorhodospira halophila*, *Biochemistry 42*, 3319−3325.
47. Baldwin, R. L. (1996) How Hofmeister ion interactions affect protein stability, *Biophys. J. 71*, 2056−2063.
48. Harper, S. M., Neil, L. C., and Gardner, K. H. (2003) Structural basis of a phototropin light switch, *Science 301*, 1541−1544.
49. Harper, S. M., Christie, J. M., and Gardner, K. H. (2004) Disruption of the LOV-J_α helix interaction activates phototropin kinase activity, *Biochemistry 43*, 16184−16192.
50. Shimizu, N., Kamikubo, H., Mihara, K., Imamoto, Y., and Kataoka, M. (2002) Effect of organic anions on the photoreaction of photoactive yellow protein, *J. Biochem. (Tokyo) 132*, 257−263.
51. Vogel, R., Fan, G.-B., Siebert, F., and Sheves, M. (2001) Anions stabilize a metarhodopsin II-like photoproduct with a protonated Schiff base, *Biochemistry 40*, 13342−13352.
52. Dickopf, S., Mielke, T., and Heyn, M. P. (1998) Kinetics of the light-induced proton translocation associated with the pH-dependent formation of the metarhodopsin I/II equilibrium of bovine rhodopsin, *Biochemistry 37*, 16888−16897.
53. Vogel, R. (2004) Influence of salts on rhodopsin photoproduct equilibria and protein stability, *Curr. Opin. Colloid Interface Sci. 9*, 133−138.
54. Farrens, D. L., Altenbach, C., Yang, K., Hubbell, W. L., and Khorana, H. G. (1996) Requirement of rigid-body motion of transmembrane helices for light activation of rhodopsin, *Science 274*, 768−770.
55. Sheikh, S. P., Zvyaga, T. A., Lichtarge, O., Sakmar, T. P., and Bourne, H. R. (1996) Rhodopsin activation blocked by metal-ion-binding sites linking transmembrane helices C and F, *Nature 383*, 347−350.
56. Ghadouni, P., Steenhuis, J. J., Farrens, D. L., and Kobilka, B. K. (2001) Agonist-induced conformational changes in the G-protein-coupling domain of the β2 adrenergic receptor, *Proc. Natl. Acad. Sci. U.S.A. 98*, 5997−6002.
57. Ballesteros, J. A., Jensen, A. D., Liapakis, G., Rasmussen, S. G., Shi, L., Gether, U., and Javitch, J. A. (2001) Activation of the β2 adrenergic receptor involves disruption of an ionic lock between the cytoplasmic ends of transmembrane segments 3 and 6, *J. Biol. Chem. 276*, 27171−27177.
58. Shapiro, D. A., Kristiansen, K., Weiner, D. M., Kroeze, W. K., and Roth, B. L. (2002) Evidence for a model of agonist-induced activation of 5-hydroxytryptamine 2A serotonin receptors that involves the disruption of a strong ionic interaction between helices 3 and 6, *J. Biol. Chem. 277*, 11441−11449.

BI050991Z